Electronic Supporting Information

Copper(I) complexes as alternatives to iridium(III) complexes for highly efficient oxygen sensing

Santiago Medina-Rodríguez,[a,b] Francisco J. Orriach-Fernández,[b] Christopher Poole,[c] Prashant Kumar,[c] Ángel de la Torre-Vega,*[,a] Jorge Fernando Fernández-Sánchez,*[,b] Etienne Baranoff,*[,c] Alberto Fernández-Gutiérrez[b]

[a]*Department of Signal Theory, Networking and Communications, CITIC-UGR, University of Granada, C/ Periodista Rafael Gómez 2, E-18071 Granada, Spain.*

[b]*Department of Analytical Chemistry, Faculty of Sciences, University of Granada, Avda. Fuentenueva s/n, E-18071 Granada, Spain.*

[c]*School of Chemistry, University of Birmingham, Edgbaston, B15 2TT, England.*

Keywords: Cu(I) complexes, optical sensing, trace oxygen, phase-resolved, LED, phase-shift measurement

* Corresponding authors. Tel.: +34 958 240451; fax: +34 958243328.

E-mail addresses: jffernan@ugr.es (J.F. Fernández-Sánchez), atv@ugr.es (A. de la Torre-Vega), e.baranoff@bham.ac.uk (E. Baranoff)

Index

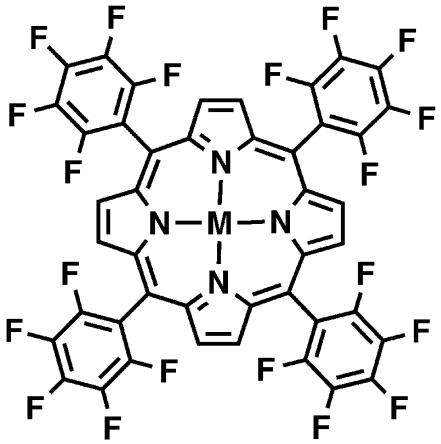

M = Pd: **PdTFPP**
M = Pt: **PtTFPP**

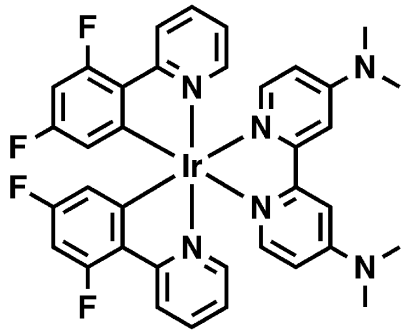

N969

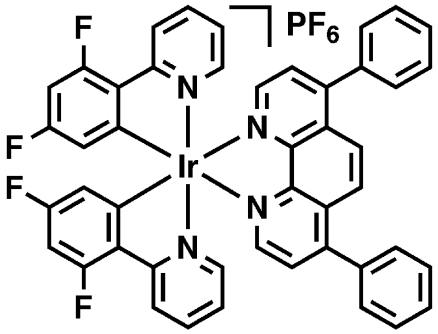

N1008

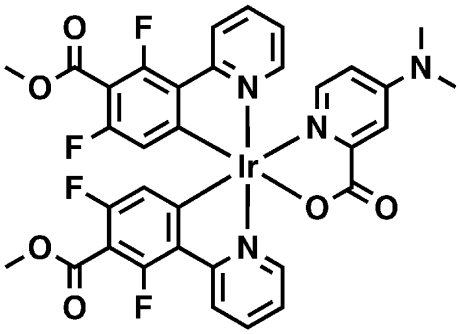

EB146

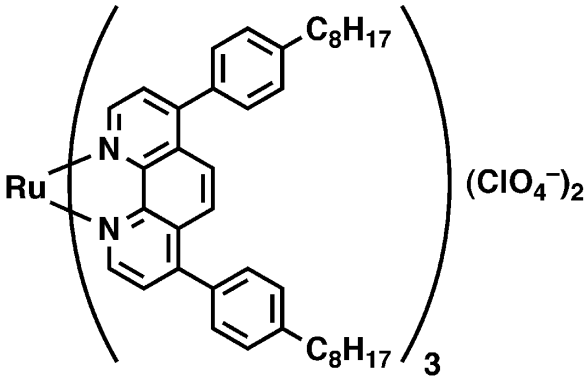

ETH^{T}-3003

Fig. S1 Chemical structure of the Pt(II), Pd(II), Ru(II), and Ir(III) complexes commented in this work.

Materials

Polystyrene (PS) was obtained from Scientific Polymers, and AP200/19 metal oxide support was prepared by Ilford Imaging Switzerland following the procedure previously published.[1-3]

Chloroform was obtained from Fluka, which was used as an organic solvent due to its good properties to dissolve the dyes. Nitrogen and oxygen (all of 99.999% purity) were obtained from Air Liquid.

Preparation of the oxygen-sensing films

The cocktails were prepared by dissolving **1**, **2** or **3** into 2 mL of chloroform (dye concentration of 1.5 mg mL^{-1}). In the case of polystyrene films, 200 mg of the polymer (PS) were added to each cocktail. The cocktails were shaken on an IKA-Vibramax-VXR (IKA-Labortechnik, Staufen, Germany) until the dye was completely dissolved. The oxygen-sensitive membranes were obtained using a Laurell spin-coater (WS-400B-6NPP/LITE, Laurell Technologies). For the AP200/19 membranes, 100 µL of the cocktail were injected onto the rotating metal oxide support fixed onto a spinning device at 300 rpm. For the PS membranes, 300 µL of the cocktail were injected onto the rotating glass support fixed onto a spinning device at 700 rpm. All membranes obtained were translucent, allowing some visible light to pass through them. The thicknesses of the sensing films were measured by SEM: AP200/19 membranes were 20 µm and PS membranes were between 2 and 7 µm in thickness after drying.

Three replicas were prepared for each membrane to evaluate the error. All the experimental results were expressed as the average of 3 repetitions ± error ($s \cdot t/\sqrt{n}$), where *s* is the standard deviation, *t* is the Student's t, and *n* is the number of repetitions.

Instruments and methods

The control of oxygen was carried out with a gas-station developed at our laboratories based on two mass flow controllers (MFC) of Type EL-FLOW® model F-201CV Bronkhorst High-Tech. Copper and stainless steel tubing was used to connect the MFCs with the self-built flow-through cell as previously reported.[4] This gas-station was controlled by a LabView 8.2 program connected to a Flow Bus interface (Bronkhorst) that completely controls the Bronkhorst mass-flow controllers via RS-232.

Excitation and emission spectra as well as intensity measurements were acquired on a Varian Cary-Eclipse luminescence spectrometer (Varian Inc.-Agilent Technologies). Lifetime measurements were carried out with the multifrequency measurement system developed by our research group.[5, 6] It uses an ultraviolet LED as light source (Ocean Optics, LED-375, λ_{max} = 375 nm, angle of illumination 15º, LED diameter 5 mm, luminous power 25 μW) filtered through an optical band-pass filter (Thorlabs GmbH, MF390-18, $\lambda_{central}$ = 390 nm). This LED is modulated by a rectangular-wave signal with 10% duty cycle at appropriate modulation frequency. The excitation signal is numerically generated with a computer and is provided by the analogue output channel on an AD/DA board (NI PCIe-6363/ BNC-2120, National Instruments, USA) at a sampling rate of 500 kS/s. This excitation signal is applied to the LED driving circuit in order to modulate the current in the LED. The voltage in a resistor in series with the LED is used as reference excitation signal. The emission signal is transduced with a photomultiplier tube (PMT) with a bandwidth dc-1 MHz (H10723-20, Hamamatsu Photonics, Japan) equipped with an appropriate optical band-pass filter, and the PMT output is amplified and filtered with appropriate analogue electronics. Both the excitation signal (the reference) and the emission signal from the sensing film are simultaneously digitized via a digital oscilloscope WaveRunner 604Zi (LeCroy, USA) at 500 kS/s using signals of 1 s in duration (i.e., a 500 kS data buffer). The bandwidth of the electronic devices and the sampling rates are large enough for the

frequency of the harmonics involved in these experiments and they are also appropriate for the typical lifetimes of the used complexes (that is, for lifetimes in the range of tens of microseconds).

All measurements were performed at room temperature (21 ºC). The temperature was continuously monitored using a commercial temperature sensor (MicroLite, Fourtec-Fourier Technologies).

Characterization of oxygen sensing films

The luminescence quantum yield, Φ, was determined following the procedure previously described in the literature for similar sensing films[1] using Ir(2-(2,4-difluorophenyl)pyridine)$_2$(4,7-diphenyl-1,10-phenanthroline)](PF_6),[2] named N1008, as reference substance ($\lambda_{exc/em}$= 400/538, Φ=0.92 ± 0.05).[2]

A standard protocol was used for characterizing the membranes.[6] To obtain the Stern-Volmer Plot (SVP), the oxygen partial pressures were calculated from the measured oxygen/nitrogen flows, assuming a constant environmental pressure of 100 kPa. Intensity and lifetime measurements were made at 14 different oxygen partial pressures between 0 and 100 kPa.

Luminescence quenching methods are based on the decrease in luminescence intensity or lifetime in the presence of the quencher (oxygen), and they are described by the Stern-Volmer equation.[7]

For complex scenarios the luminophores may exhibit characteristic quenching constants that are associated with distinct luminophore sites and/or microdomains.[6] When two microdomains are expected, the experimental data can be fitted using a two-site model proposed by Demas and co-workers, and called the Demas model.[8] The Stern-Volmer constants are calculated with the next expression:

$$\frac{I_0}{I} = \frac{\tau_0}{\tau} = \left[\frac{x_1}{1 + K_{SV,1} \cdot pO_2} + \frac{x_2}{1 + K_{SV,2} \cdot pO_2} \right]^{-1}$$

where I is the luminescence intensity, τ is the luminescence lifetime, the subindex 0 represents unquenched conditions, and x_i denotes the fractional contribution of the total luminescence emission from the luminophore located at site type i, which exhibits a discrete Stern-Volmer quenching constant given by $K_{SV,i}$.

The apparent luminescence lifetimes were determined by phase-resolved luminescence[7] using a multifrequency phase-modulation method that uses rectangular-wave signals with a short duty cycle to modulate the excitation light source.[6] Luminescence from a monoexponential luminophore using an excitation modulated at a frequency (f) presents a luminescence phase-shift $\phi(f)$ described by:

$$\phi(f) = -\arctan\,(2\pi f \tau_\phi)$$

From this equation, the phase-shift based apparent lifetime can be estimated at frequency f as:

$$\tau_\phi(f) = \tan\big(-\phi(f)\big)\,/2\pi f$$

In this work, the use of short duty-cycle rectangular signals for excitation provides several harmonics with enough amplitude for allowing the simultaneous measurement of phase shift and modulation factor at several frequencies. For multifrequency analysis of the luminescent response, we propose an analogue-to-digital conversion and subsequent processing of the recorded digital signal, which can easily be implemented via software in a conventional computer or a microcontroller.[6]

Table S1 Luminescent properties of the complexes; Φ is the luminescence quantum yield and τ_0 is the luminescent lifetime in absence of oxygen.

Sensing film	λ_{exc} (nm)	λ_{em} (nm)	Φ	τ_0 (μs)
1-PS	375	500	0.290	26.0
1-AP200/19	376	518	0.293	22.5
2-PS	288	500	0.221	—
2-AP200/19	338	500	0.113	—
3-PS	296	496	—	—
3-AP200/19	308	550	—	—

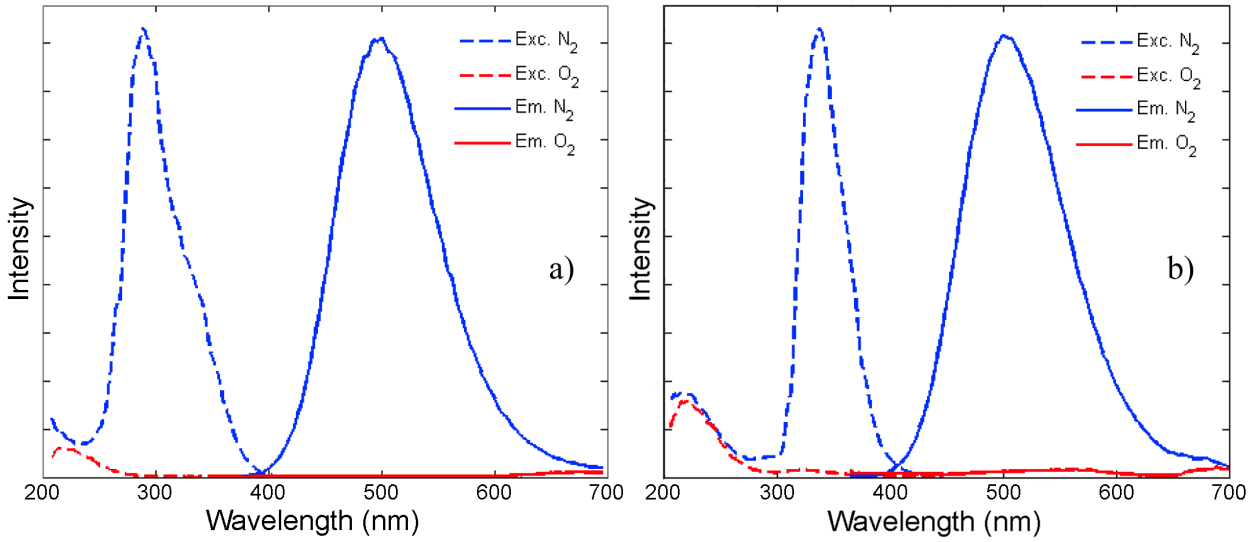

Fig. S2 Excitation (---) and emission (—) spectra of a) **2**-PS and b) **2**-AP200/19 in the presence (red) and absence (blue) of oxygen.

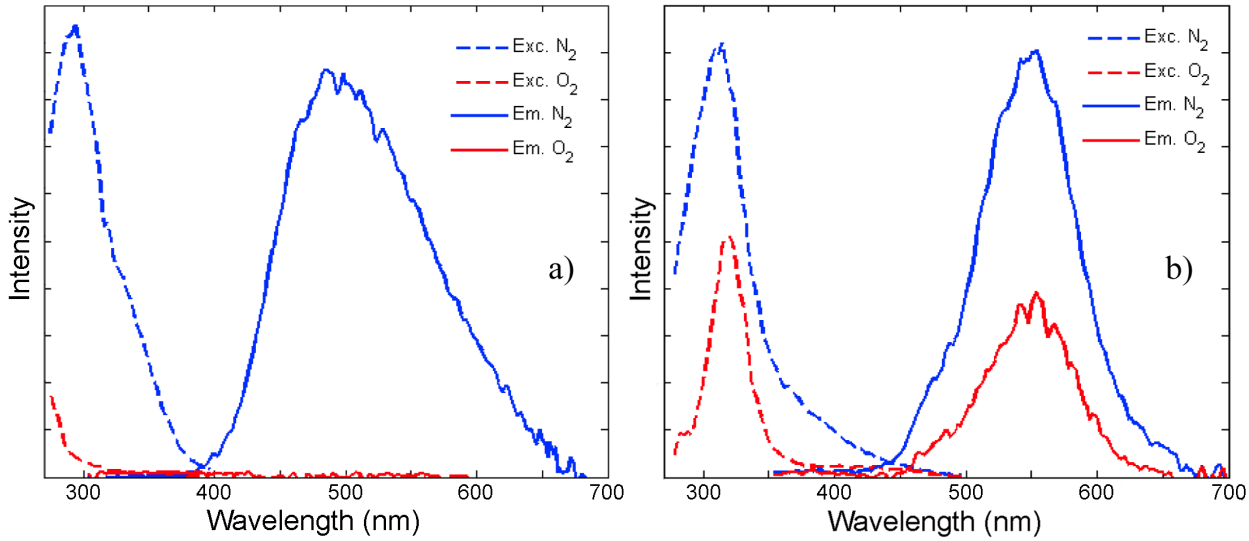

Fig. S3 Excitation (---) and emission (—) spectra of a) **3**-PS and b) **3**-AP200/19 in the presence (red) and absence (blue) of oxygen.

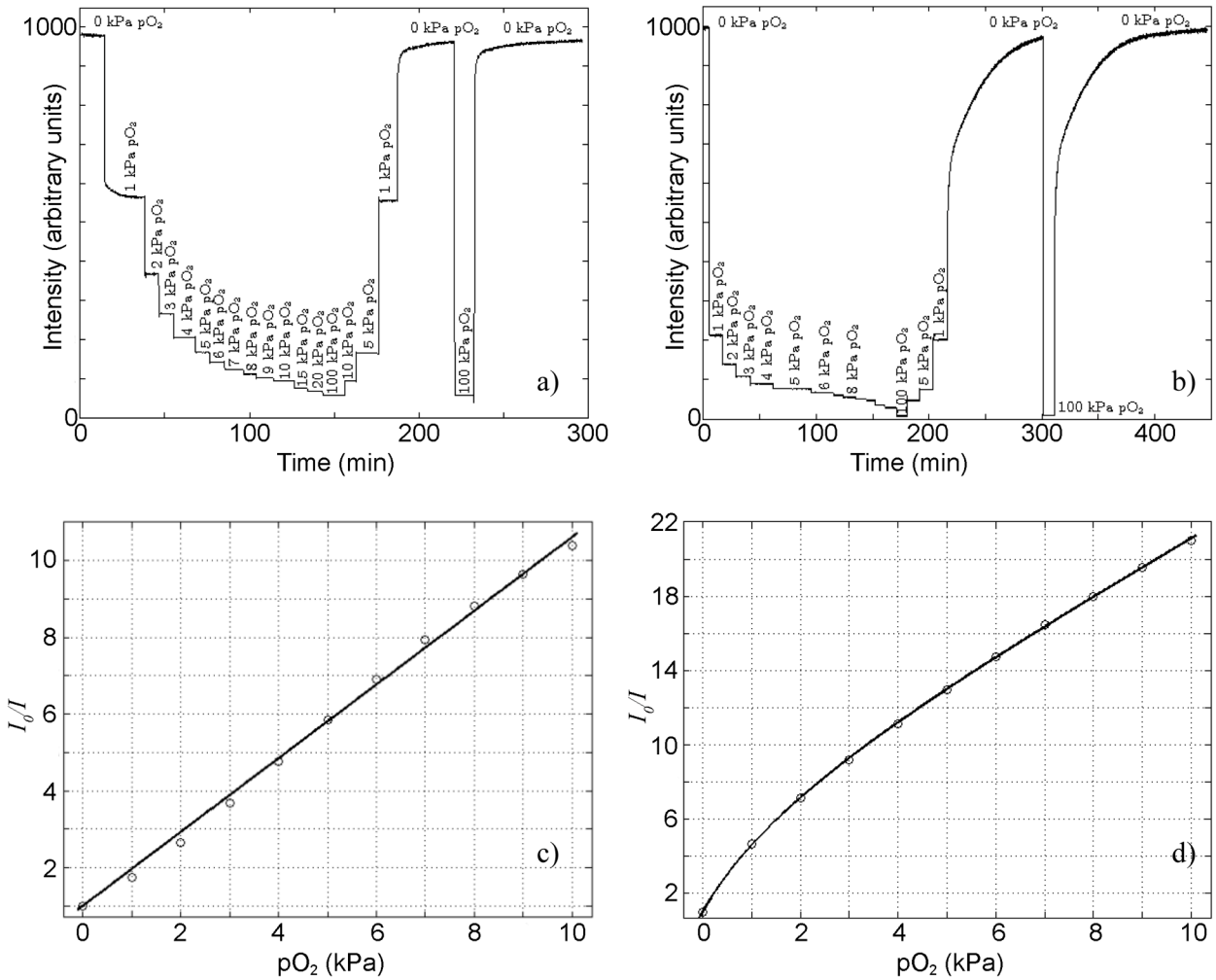

Fig. S4 Time trace curves (variation of the luminescence intensity with the oxygen concentration) for a) **1**-PS and b) **1**-AP200/19, and Stern-Volmer plots in the range 0-10 kPa O_2 for c) **1**-PS and d) **1**-AP200/19 obtained by intensity measurements (Fig. S4c,d are as Fig. 3a,b in main text; reproduced here for convenience).

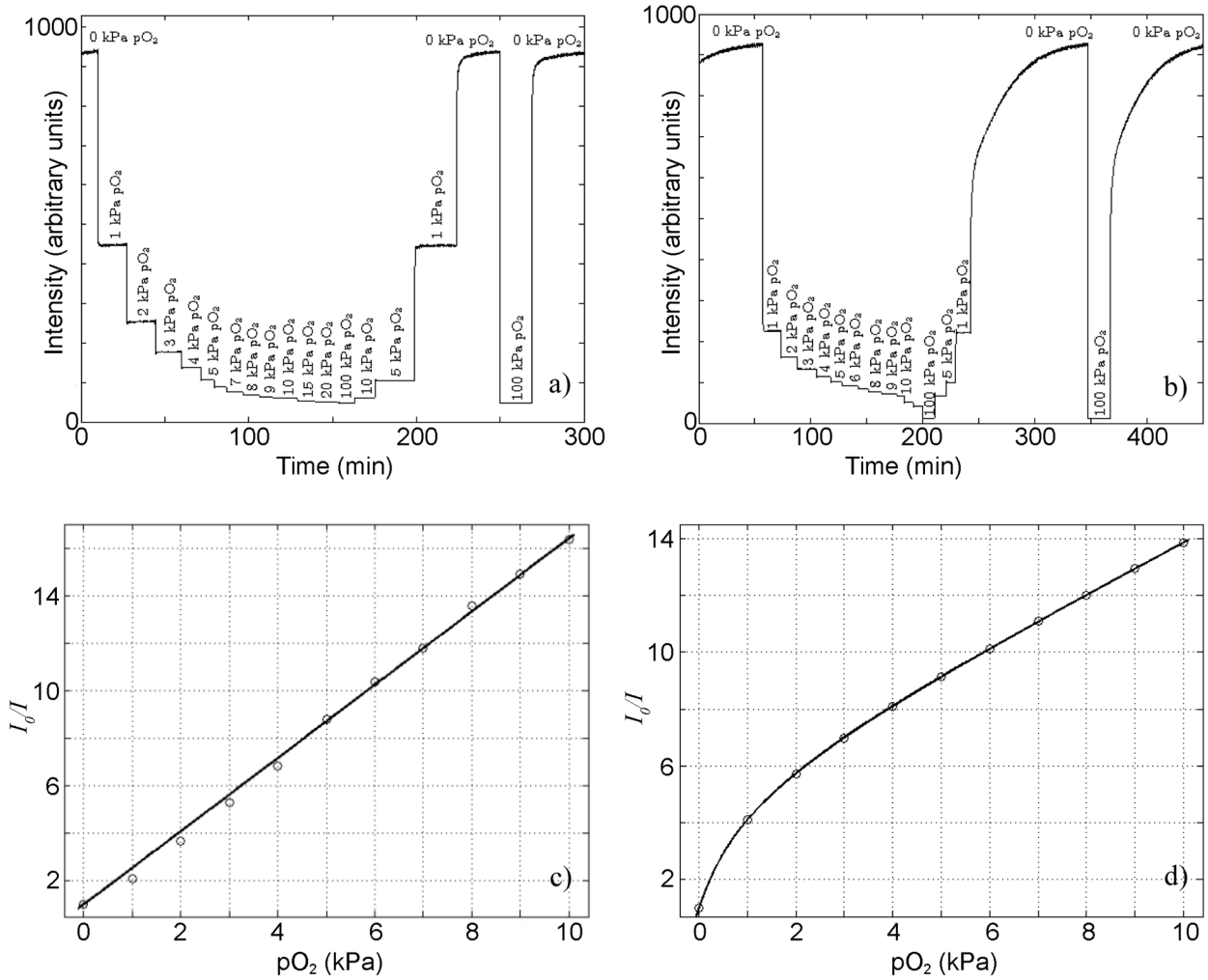

Fig. S5 Time trace curves (variation of the luminescence intensity with the oxygen concentration) for a) **2**-PS and b) **2**-AP200/19, and Stern-Volmer plots in the range 0-10 kPa pO_2 for c) **2**-PS and d) **2**-AP200/19 obtained by intensity measurements.

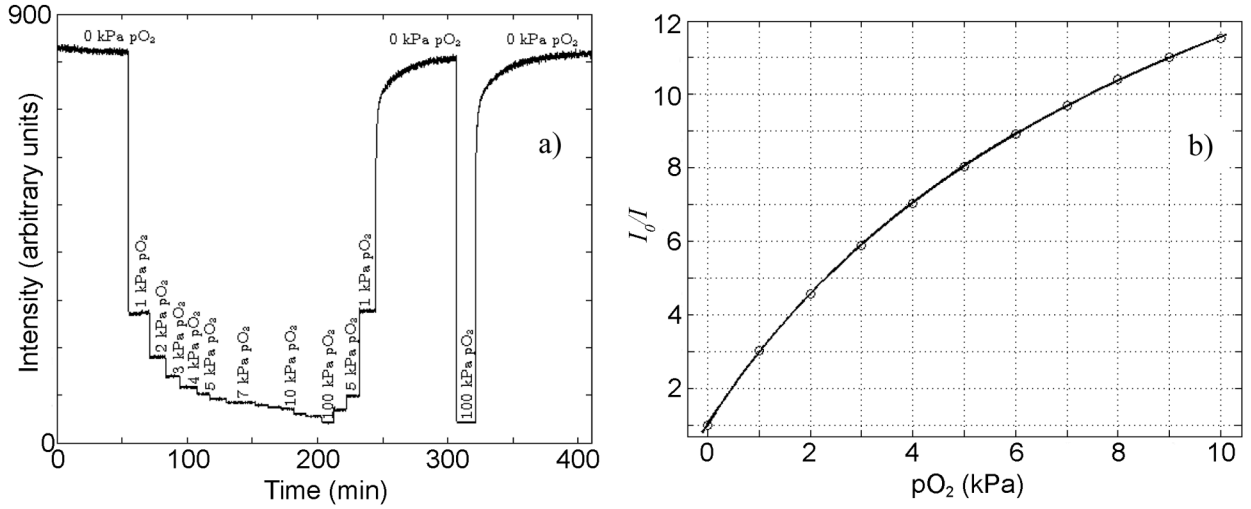

Fig. S6 a) Time trace curves (variation of the luminescence intensity with the oxygen concentration) for **3**-PS and b) Stern-Volmer plots in the range 0-10 kPa pO_2 for **3**-PS.

Table S2 Oxygen sensitivity of sensing films using luminescence intensity measurements.

Range	Parameters	Intensity measurements* (I_0/I)		
		2-PS	**2**- AP200/19	**3**-PS
0-10 kPa pO_2	K_{SV1} (kPa^{-1})	1.590 ± 0.110[a]	5.130 ± 0.192[b]	2.570 ± 0.161[b]
	x_1	1.0 ± 0.0	0.88 ± 0.05	0.93 ± 0.09
	K_{SV2} (kPa^{-1})	–	0.100 ± 0.008	0.040 ± 0.014
	x_2	–	0.12 ± 0.04	0.07 ± 0.12
	R^2	0.9914 ± 0.0139	0.9960 ± 0.0115	0.9977 ± 0.0068
0-100 kPa pO_2	K_{SV1} (kPa^{-1})	3.149 ± 0.125[b]	3.799 ± 0.170[b]	2.333 ± 0.049[b]
	x_1	0.96 ± 0.02	0.90 ± 0.01	0.95 ± 0.04
	K_{SV2} (kPa^{-1})	0.00 ± 0.00	0.0860 ± 0.0480	0.0003 ± 0.0001
	x_2	0.04 ± 0.01	0.10 ± 0.03	0.05 ± 0.01
	R^2	0.9332 ± 0.0205	0.9996 ± 0.0008	0.9985 ± 0.0051

*[Dye concentration] = 1.5 mg mL^{-1}; the results are the average of 3 replicas $\pm s\frac{t}{\sqrt{n}}$ (n = 3, t = 4.303 (2P = 0.05), s = standard deviation); [a] Data fitted with the Stern-Volmer model; [b] Data fitted with the Demas two-site model.

Mutifrequency analysis

For multifrequency analysis, rectangular-wave excitation signals with a 10% duty cycle and different fundamental frequencies (i.e., 113, 565 and 2825 Hz) were used to set the modulation frequency for each sensing film. The procedure for the selection of the modulation frequency can be found in reference.[9]

This study (see Fig. S7 and S8 below) concludes that the most suitable modulation frequencies (in the frequency range 100 Hz - 23 kHz) for the measurement range 0-10 kPa pO_2 are 5650 Hz for the 1-PS sensing film (average phase difference of 21.83º) and 14125 Hz for the 1-AP200/19 sensing film (average phase difference of 37.28º). Similar modulation frequencies were obtained for the measurement range 0-1 kPa pO_2. After finding the appropriate modulation frequency for each sensing film, 10% duty cycle rectangular-wave excitation signals with the selected modulation frequencies (i.e., with fundamental frequencies of 5650 Hz and 14125 Hz for 1-PS and 1-AP200/19 membranes, respectively) were used to carry out the calibration of the sensing films. This allowed a higher power of

signalling (i.e., better signal-to-noise ratio (SNR) for the modulated signal), since the first harmonic of the rectangular signal (the fundamental harmonic) has the greatest amplitude.[6]

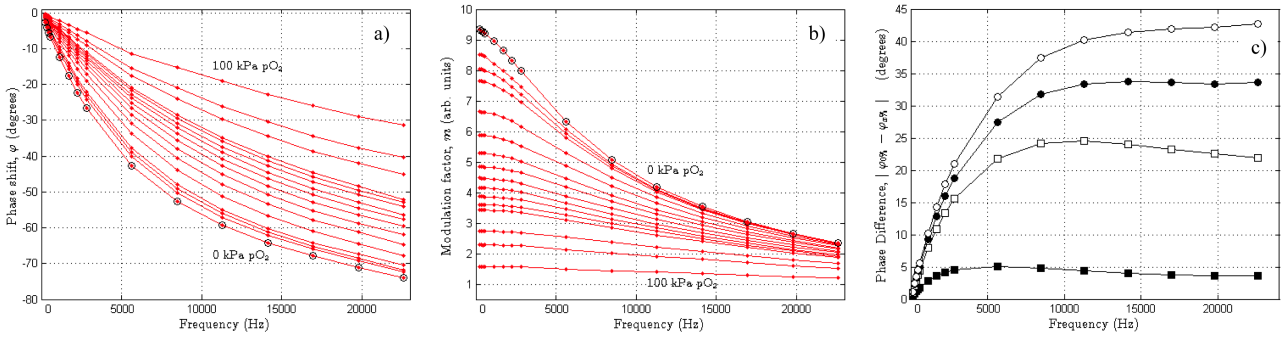

Fig. S7 Variation of the a) phase-shift and b) modulation factor[a] with the modulation frequency at different oxygen concentrations (0, 0.5, 0.75, 1, 2, 3, 4, 5, 6, 7, 8, 9, 10, 15, 20 and 100 kPa pO_2), and c) effect of the modulation frequency on the average phase difference at several oxygen concentrations (■ from 0 to 1 kPa pO_2, □ from 0 to 10 kPa pO_2, ● from 0 to 20 kPa pO_2, ○ from 0 to 100 kPa pO_2) of **1**-PS at 21 ºC.

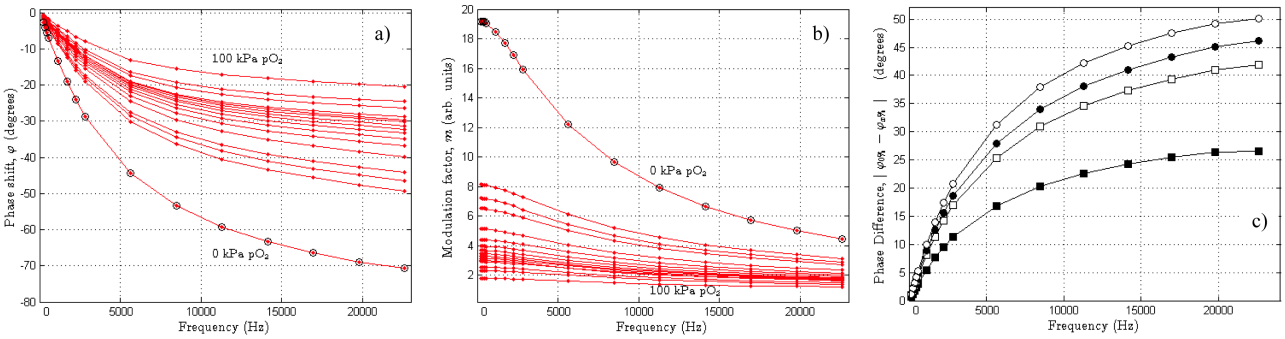

Fig. S8 Variation of the a) phase-shift and b) modulation factor[a] with the modulation frequency at different oxygen concentrations (0, 0.5, 0.75, 1, 2, 3, 4, 5, 6, 7, 8, 9, 10, 15, 20 and 100 kPa pO_2), and c) effect of the modulation frequency on the average phase difference at several oxygen concentrations (■ from 0 to 1 kPa pO_2, □ from 0 to 10 kPa pO_2, ● from 0 to 20 kPa pO_2, ○ from 0 to 100 kPa pO_2) of **1**-AP200/19 at 21 ºC.

[a] Modulation factors are estimated from the measurements at both channels of the digital oscilloscope (see reference 6). The amplitude of the excitation signal is expressed in volts and the emission signal is also expressed in volts after transduction in the Photomultiplier Tube (PMT) and preamplification. So, modulation factor is expressed in V/V, even though the values would be scaled depending on the configuration of the PMT and the preamplification stage. For this reason, the modulation factor is expressed in arbitrary units.

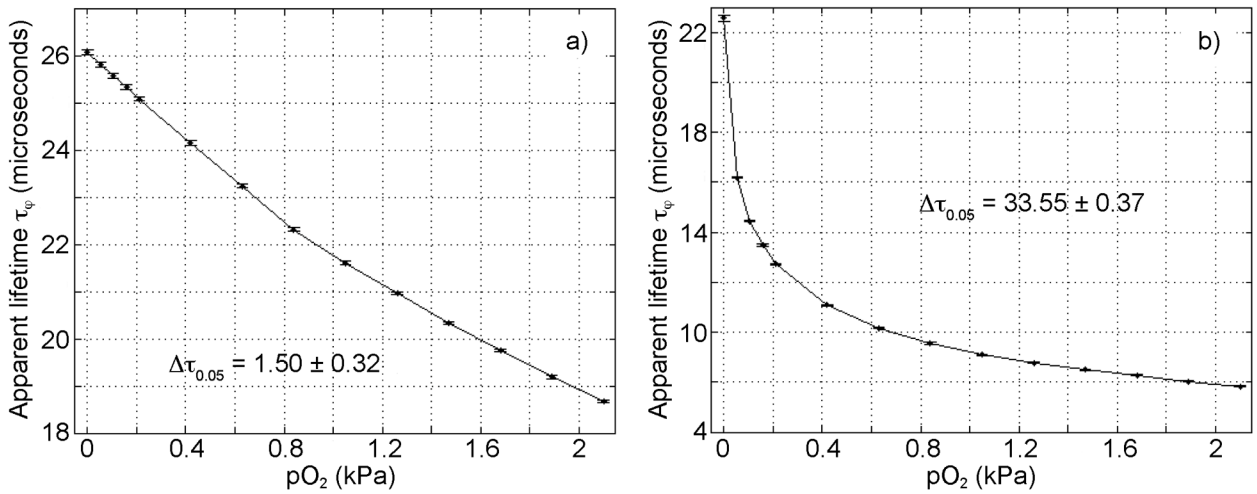

Fig. S9 Variation of the apparent lifetime between 0 and 2.1 kPa pO_2 of a) **1**-PS and b) **1**-AP200/19 at 21 ºC and the parameter $\Delta_{\tau_{0.05}}$.

Table S3 Measurement capability of the developed sensing films using luminescence intensity measurements and apparent luminescence lifetime measurements determined from the phase shift. The data are shown in kPa and the relative error (into bracket) in %.

	Intensity measurements[a]				
Real pO_2, kPa	**1**-PS	**1**-AP200/19	**2**-PS	**2**-AP200/19	**3**-PS
1.00	0.917 (9.72)	1.023 (2.43)	0.902 (9.92)	1.000 (0.18)	1.020 (2.22)
2.00	1.840 (8.55)	1.997 (0.31)	1.854 (7.73)	1.998 (0.23)	1.998 (0.42)
3.00	2.904 (6.57)	2.973 (0.96)	2.902 (6.66)	3.000 (0.18)	2.995 (0.58)
5.00	5.047 (0.98)	4.984 (0.43)	5.042 (0.87)	5.001 (0.14)	4.987 (0.97)
6.00	6.143 (2.41)	6.008 (0.28)	6.083 (1.41)	5.999 (0.20)	5.993 (0.89)
7.00	7.204 (2.95)	7.040 (0.62)	7.005 (0.14)	7.004 (0.22)	7.003 (0.88)
9.00	9.001 (0.10)	8.996 (0.22)	9.013 (0.18)	9.001 (0.18)	8.990 (0.79)

	Lifetime measurements[b]	
Real pO_2, kPa	**1**-PS	**1**-AP200/19
0.50	0.479 (3.25)	0.523 (3.64)
0.75	0.744 (1.19)	0.748 (0.92)
1.00	0.999 (1.06)	0.972 (2.83)
3.00	2.999 (0.52)	2.975 (1.34)
5.00	5.001 (0.53)	5.050 (1.55)
6.00	5.970 (0.74)	6.028 (1.80)
7.00	7.009 (0.68)	7.036 (1.48)
9.00	9.093 (1.15)	8.959 (1.51)

[a] All values correspond to the average of 50 measurements. Calibration curves obtained for the luminescence intensity (*I*, expressed in arbitrary units) in the range of 0-10 kPa pO_2 were used.
[b] All values correspond to the average of 50 measurements. Calibration curves obtained for the apparent lifetime determined from the phase-shift (τ_φ, expressed in microseconds) at a single modulation frequency in the range of 0-10 kPa pO_2 were used.

Table S4 Response times (t_{95}) of the dyes incorporated into PS and AP200/19.

	t_{95} Response time (s)	
Sensing film*	1-5 kPa	5-1 kPa
1-PS	10.0 ± 0.5	13.0 ± 0.4
1-AP200/19	3.3 ± 0.3	10.4 ± 0.5
2-PS	6.4 ± 0.3	11.1 ± 0.6
2-AP200/19	5.8 ± 0.4	10.7 ± 0.5
3-PS	11.0 ± 0.3	15.6 ± 0.4

*[Dye concentration] = 1.5 mg mL^{-1}; the results are the average of 3 replicas $\pm s\frac{t}{\sqrt{n}}$ (n = 3, t = 4.303 (2P = 0.05), s = standard deviation). Time curse curves are shown in Fig. S4 to S6.

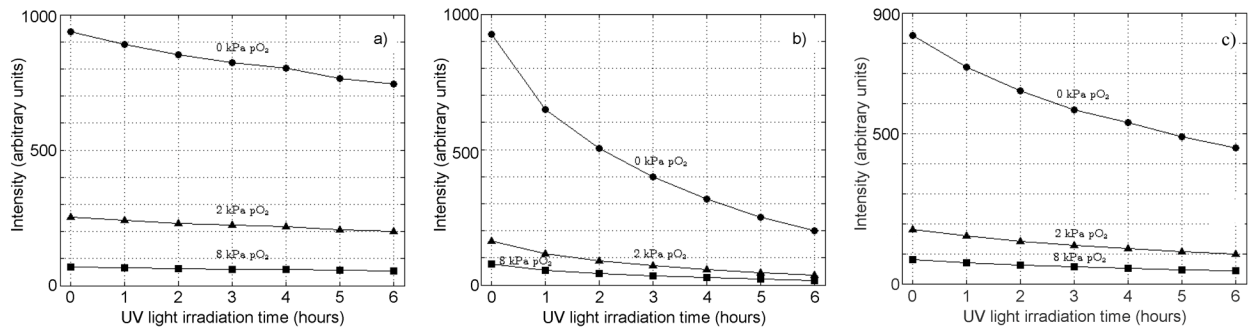

Fig. S10 Photostability testing of a) **2**-PS, b) **2**-AP200/19 and c) **3**-PS at 21 ºC for several oxygen concentrations using intensity measurements (● 0 kPa pO_2; ▲ 2 kPa pO_2; ■ 8 kPa pO_2).

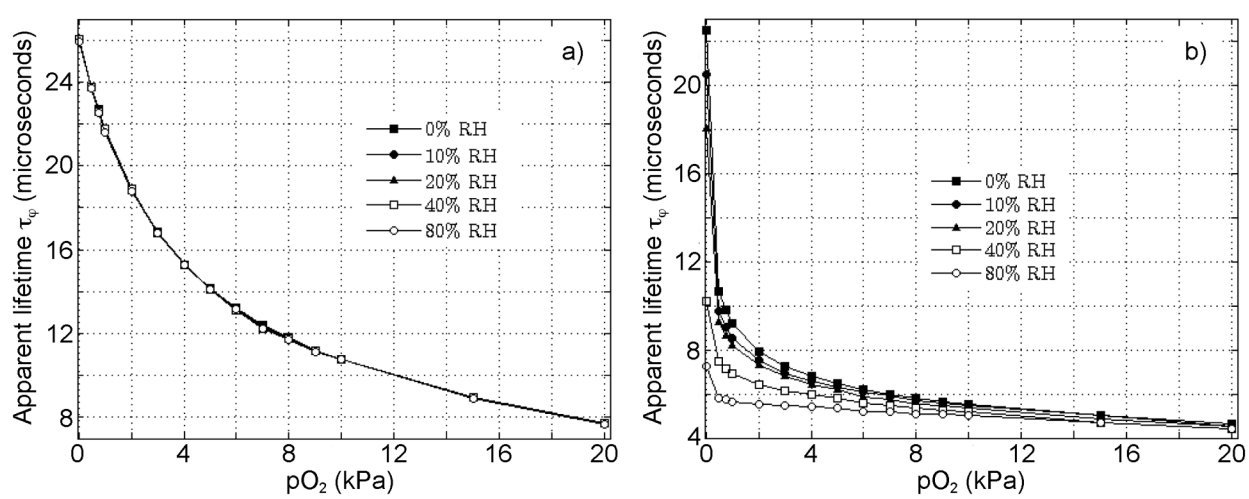

Fig. S11 Effect of relative humidity (RH, %) on the apparent lifetime estimated from phase shift (τ_{φ}, expressed in microseconds) of a) **1**-PS and b) **1**-AP200/19 at 21 ºC.

Characterisation of complexes

The data show that no major impurity (such as free ligand or unwanted homoleptic complexes made from dynamic ligand exchange reaction in solution, see ref. 10) is detected in the synthesised complexes. In particular for complex **1**, the complex $Cu(dmp)_2^+$ is not detected using ^1H NMR, MS, or UV-visible absorption, which support complexes purity >95% .

Cu(Xantphos)(dmp)(PF_6) 1

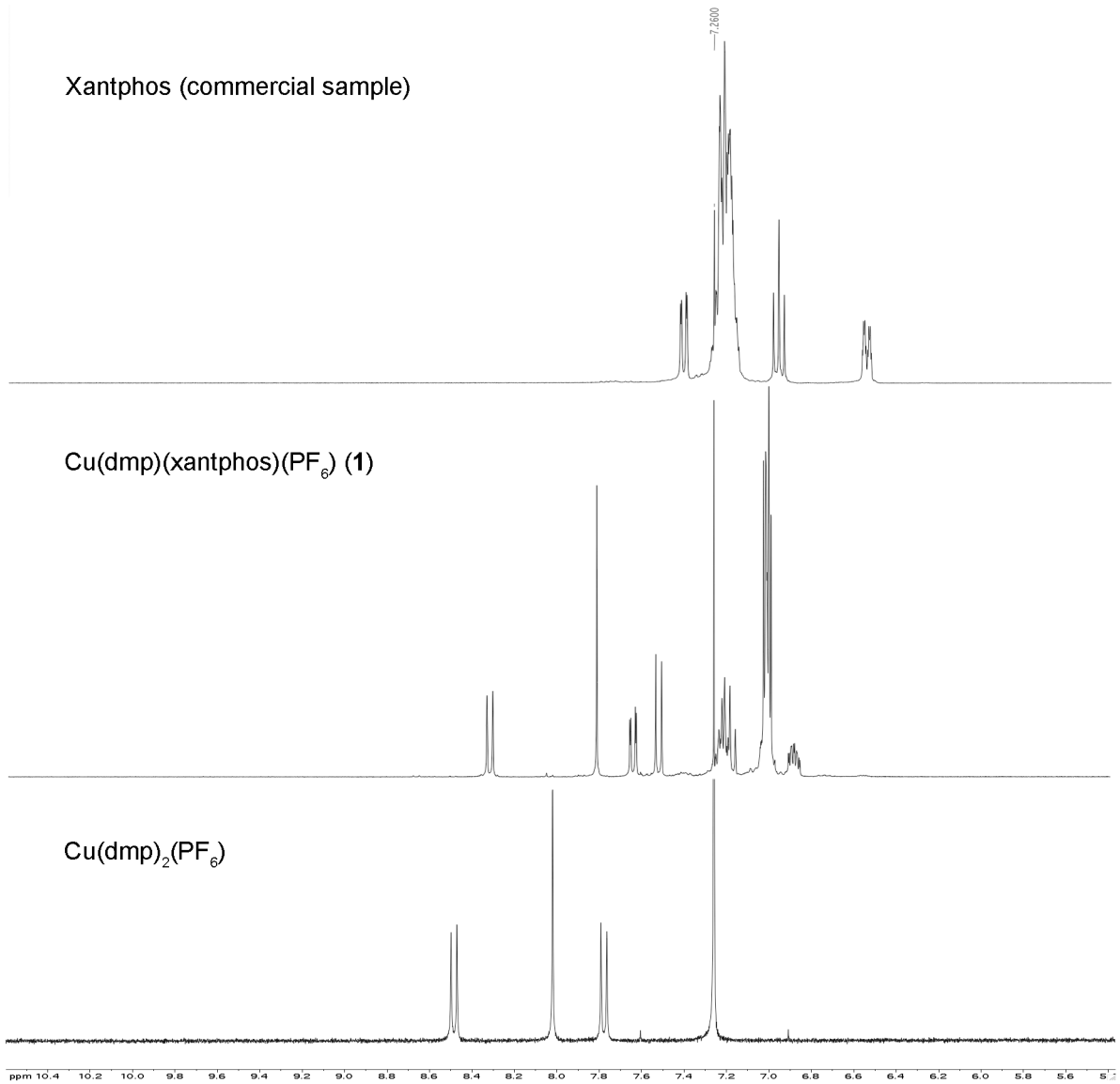

Fig. S12 Aromatic region of ^1H NMR spectra in $CDCl_3$ of **1** and free Xantphos and $Cu(dmp)_2(PF_6)$.

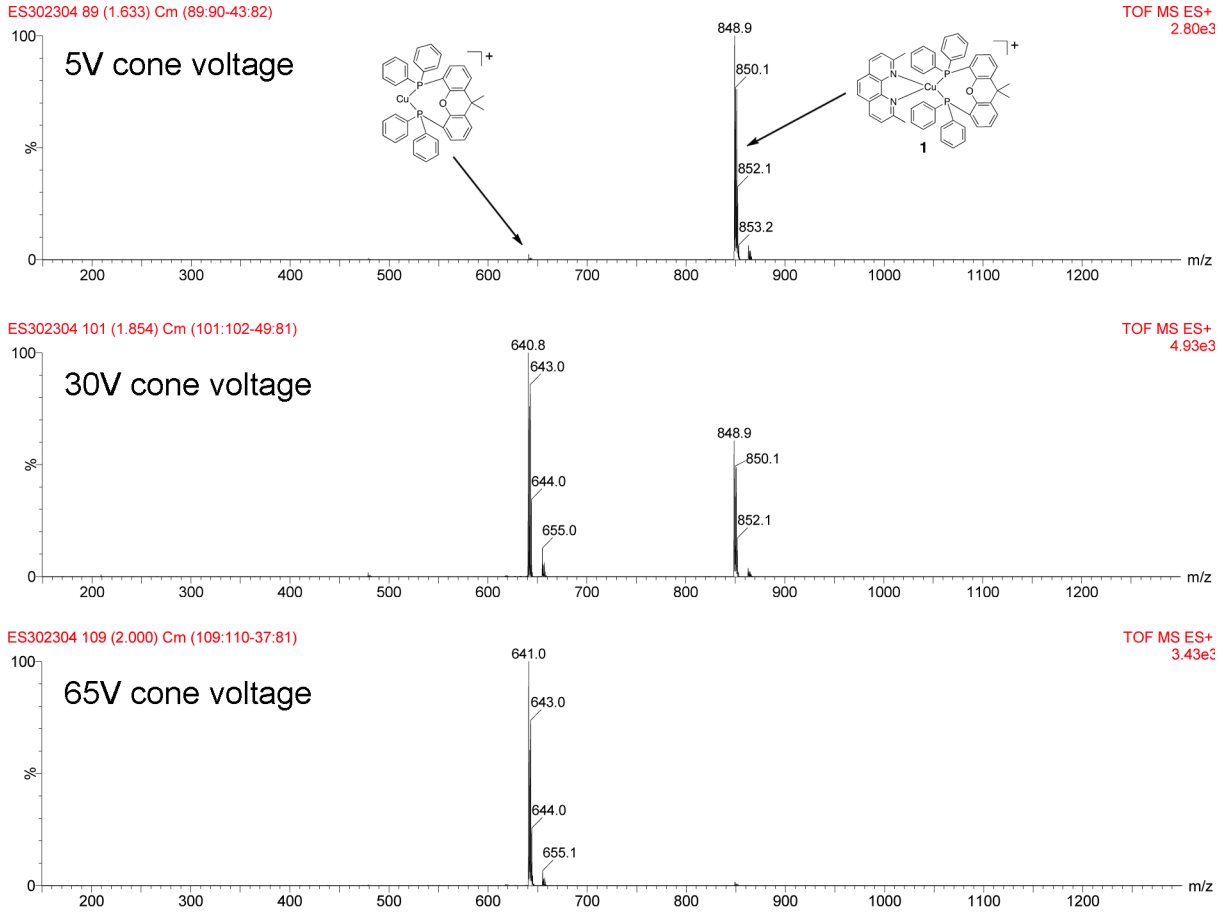

Fig. S13 Mass spectrum of **1**.

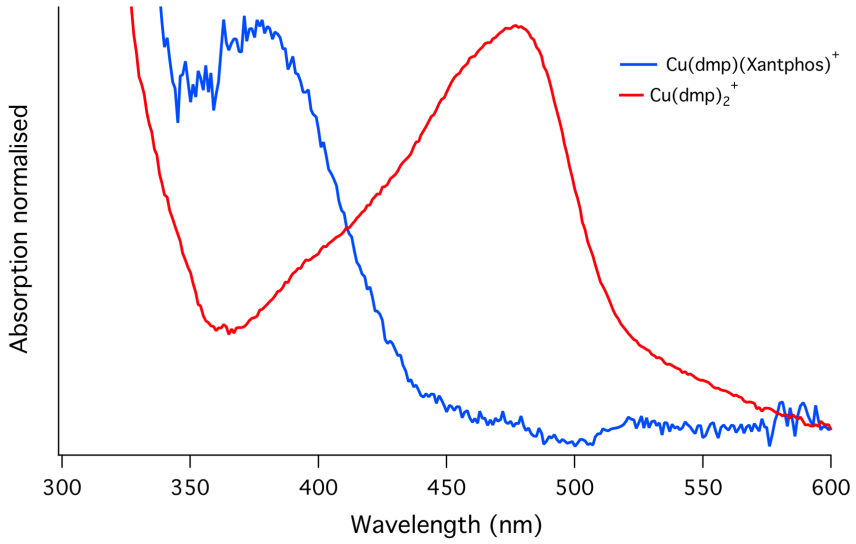

Fig. S14 Absorption spectrum of **1** (blue line) and $Cu(dmp)_2(PF_6)$ in CH_2Cl_2. The spectra are normalised to the MLCT absorption band.

Cu(Xantphos)(pzpy)(PF_6) 2

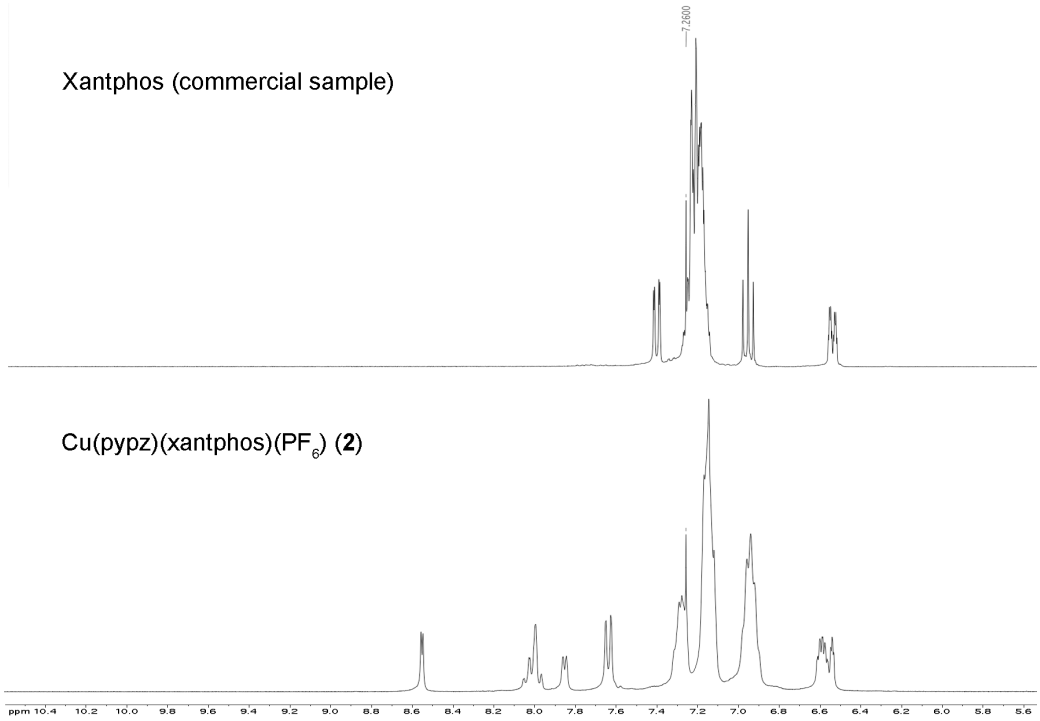

Fig. S15 Aromatic region of ^{1}H NMR spectra in $CDCl_3$ of **2** and free Xantphos.

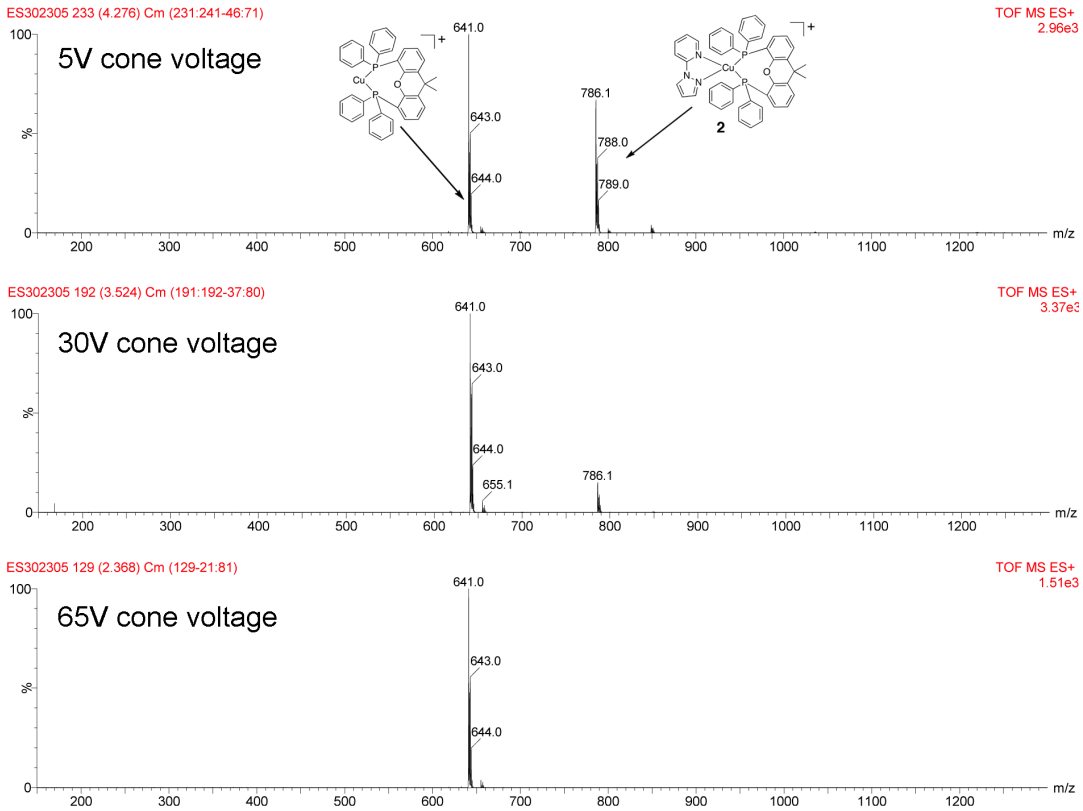

Fig. S16 Mass spectrum of **2**.

Cu(Xantphos)$_2$(PF$_6$) 3

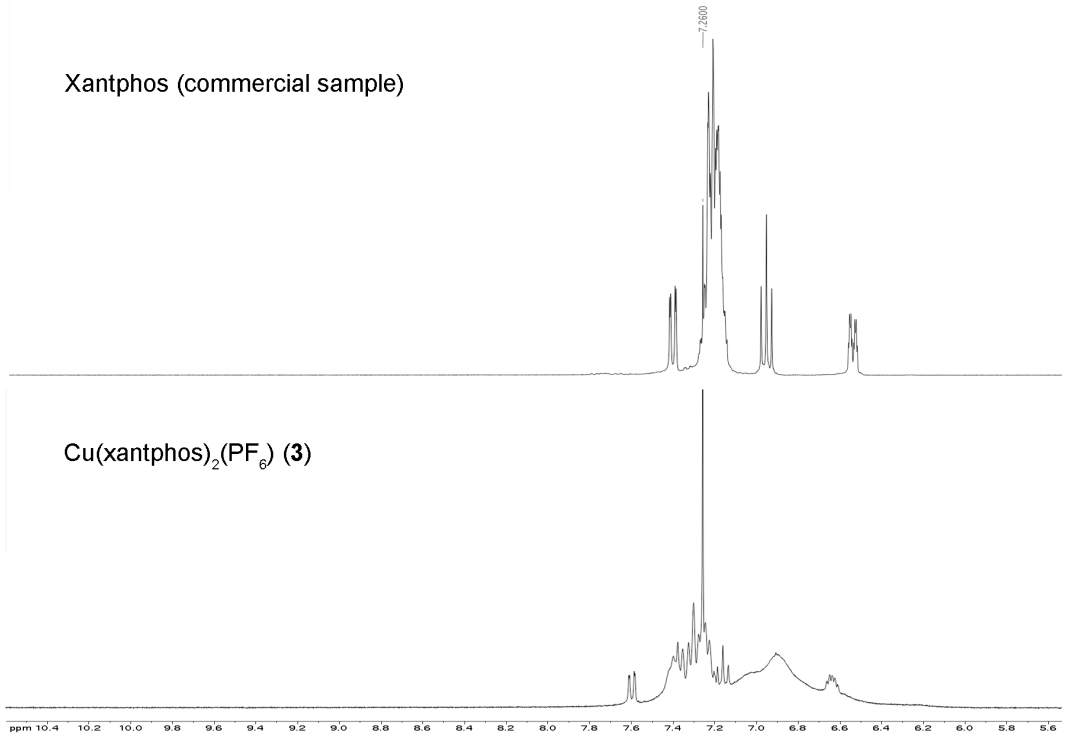

Fig. S17 Aromatic region of ^{1}H NMR spectra in $CDCl_3$ of **3** and free Xantphos.

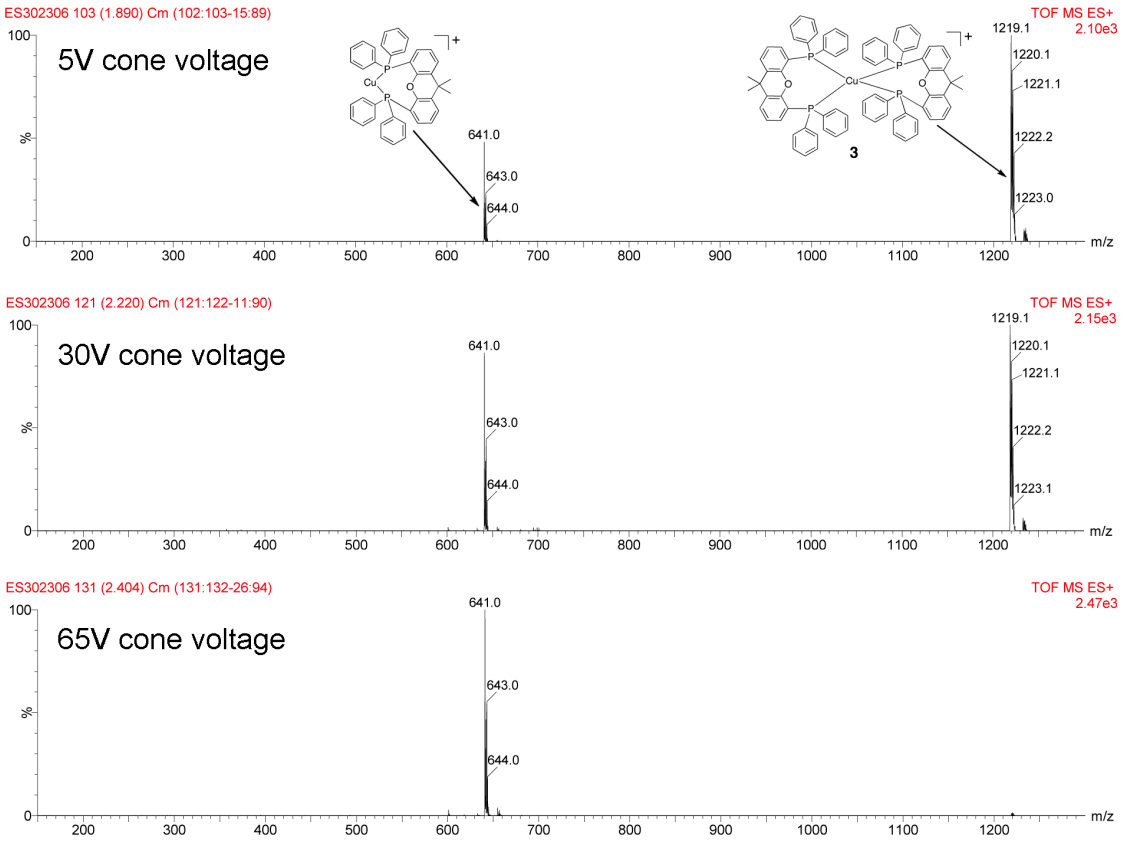

Fig. S18 Mass spectrum of **3**.

References

1. J. F. Fernández-Sánchez, R. Cannas, S. Spichiger, R. Steiger and U. E. Spichiger-Keller, *Anal. Chim. Acta*, 2006, **566**, 271-282.

2. M. Marín-Suárez del Toro, J. F. Fernández-Sánchez, E. Baranoff, M. K. Nazeeruddin, M. Gräetzel and A. Fernández-Gutiérrez, *Talanta*, 2010, **82**, 620-626.

3. J. F. Fernández-Sánchez, I. Fernández, R. Steiger, R. Beer, R. Cannas and U. E. Spichiger-Keller, *Adv. Funct. Mater.*, 2007, **17**, 1188-1198.

4. A. L. Medina-Castillo, J. F. Fernández-Sánchez, C. Klein, M. K. Nazeeruddin, A. Segura-Carretero, A. Fernández-Gutiérrez, M. Graetzel and U. E. Spichiger-Keller, *Analyst*, 2007, **132**, 929-936.

5. S. Medina-Rodríguez, A. de la Torre-Vega, J. F. Fernández-Sánchez and A. Fernández-Gutiérrez, *Sensor. Actuat. B: Chem.*, 2013, **176**, 1110-1120.

6. S. Medina-Rodríguez, A. de la Torre-Vega, F. J. Sainz-Gonzalo, M. Marín-Suárez, C. Elosúa, F. J. Arregui, I. R. Matias, J. F. Fernández-Sánchez and A. Fernández-Gutiérrez, *Anal. Chem.*, 2014, **86**, 5245-5256.

7. J. R. Lakowicz, *Principles of Fluorescence Spectroscopy*, 2nd edn., Kluwer Academic, New York, 1999.

8. J. N. Demas and B. A. DeGraff, *Sensor. Actuat. B: Chem.*, 1993, **11**, 35-41.

9. S. Medina-Rodriguez, M. Marin-Suarez, J. F. Fernandez-Sanchez, A. d. l. Torre-Vega, E. Baranoff and A. Fernandez-Gutierrez, *Analyst*, 2013, **138**, 4607-4617.

10. A. Kaeser, M. Mohankumar, J. Mohanraj, F. Monti, M. Holler, J.-J. Cid, O. Moudam, I. Nierengarten, L. Karmazin-Brelot, C. Duhayon, B. Delavaux-Nicot, N. Armaroli, J.-F. Nierengarten, *Inorg. Chem.*, 2013, **52**, 12140-12151.